LAWRENCE
LIVERMORE
NATIONAL
LABORATORY

UCRL-JRNL-204966

Measurement of 2l – nl' X-ray Transitions from Kr Clusters Irradiated by Femtosecond Laser Pulses

S. B. Hansen, K. B. Fournier, A. Ya. Faenov, A. I. Magunov, T. A. Pikuz, I. Yu. Skobelev, Y. Fukuda, Y. Akahane, M. Aoyama, N. Inoue, H. Ueda, and K. Yamakawa

6/28/2004

Submitted to Physical Review E

Measurement of 2ℓ - $n\ell'$ x-ray transitions from Kr clusters irradiated by femtosecond laser pulses

S. B. Hansen and K. B. Fournier
Lawrence Livermore National Laboratory, P.O. Box 808, L-473, Livermore, CA 94550, USA

A. Ya. Faenov, A. I. Magunov, T. A. Pikuz, and I. Yu. Skobelev
Multicharged Ions Spectra Data Center of VNIIFTRI, Mendeleevo, Moscow region 141570, Russia

Y. Fukuda, Y. Akahane, M. Aoyama, N. Inoue, H. Ueda, and K. Yamakawa
Advanced Photon Research Center, Japan Atomic Energy Research Institute (JAERI), 8-1 Umemidai, Kizu-cho, Souraku-gun, Kyoto 619-0215, Japan
(Dated: June 18, 2004)

X-ray line emission from $2\ell - n\ell'$ transitions in Ne-like Kr and nearby ions has been observed from ≈ 1 μm Kr clusters irradiated by fs-scale laser pulses at the JAERI facility in Kyoto, Japan. The incident laser intensity reached 10^{19} W/cm^2, with pulse energies from 50 to 300 mJ and pulse durations from 30 to 500 fs. The dependence of the x-ray spectral features and intensity on the incident laser intensity is rather weak, indicating that the 1 – 2 ps cluster lifetimes limit the number of ions beyond Ne-like Kr that can be produced by collisional ionization. Lines from F- to Al-like Kr emitted from the cluster plasmas have been identified using data from the relativistic multiconfiguration atomic structure code FAC. A collisional-radiative model based on this data has been constructed and used to determine that the cluster plasma has electron densities near 10^{22} cm^{-3}, temperatures of a few hundred eV and hot electron fractions of a few percent.

PACS numbers: 52.50.Jm, 32.30.Rj, 36.40.Vz, 52.25.Os

I. INTRODUCTION

Plasmas formed by the irradiation of gas clusters by short-pulse, high-intensity lasers are promising x-ray emission sources. First explained in [1], gas cluster plasmas have been extensively studied over the last few years [2–7]. Resonant laser-plasma interactions within cluster targets generate high-energy particles [2, 3] such as hot electrons, which can lead to considerable x-ray yields [4–7]. The study of cluster targets under intense laser irradiation is relevant to fusion studies [2], development of high-intensity x-ray sources [1], and investigations into the behavior of matter in ultrahigh electric fields [8].

The interaction of ultrashort laser pulses with solid targets can generate plasmas with very high electron densities [9] and significant fractions of hot electrons [10, 11], but the conversion efficiency of laser light to multi-keV x-rays from solid targets tends to be rather low. The absorption of laser light by a uniform low-density gas is inherently more efficient than by a massive, solid target [12, 13] because the laser can supersonically ionize and heat large volumes with little or no loss of energy to ablative interactions with the target far from the emitting region. For this reason, gas cluster targets [8] and low-density solid targets [14] are also efficient absorbers of laser energy.

In a previous work [5], the $2\ell - 4\ell'$ emission from Ne-like Kr and surrounding ions was analyzed and used to diagnose the conditions of ≈ 0.1 μm clusters irradiated by 60 and 500 fs laser pulses with 4 – 15 mJ of energy and intensities up to 7×10^{17} W/cm^2. Those plasmas contained hot, dense regions consisting of cluster remnants with electron densities near 10^{21} cm^{-3}, temperatures between 300 and 400 eV, and hot electron fractions of 2 – 4%. The cluster plasma regions, from which most of the L-shell x-rays were emitted, were surrounded by cooler (200 eV), rarer (10^{20} cm^{-3}) plasma formed during the laser prepulse.

In the present work, emission from 2ℓ - $n\ell'$ transitions with $n \leq 6$ is analyzed from larger Kr clusters whose dimensions are estimated to be ≈ 1 μm. The nozzle in this experiment was designed was to maximize the cluster size [15], since larger clusters have been found to be less susceptible to destruction by the laser prepulse and more efficient absorbers of the laser energy [5]. The large Kr clusters in the present experiment were irradiated by 30 – 500 fs laser pulses with 50 – 300 mJ of energy; laser intensities up to 10^{19} W/cm^2 have been achieved. The resulting L-shell Kr emission spectra indicate that the cluster plasmas reach electron densities larger than 10^{22} cm^{-3}, have temperatures near 250 eV, and hot electron fractions near 2%. It is estimated that 10 – 50 mJ from ≈ 120 mJ of incident laser energy are required to produce the cluster plasma, indicating fairly high absorption efficiencies that increase with decreasing pulse duration.

Previous measurements of 2ℓ - $n\ell'$ emission from O- to Mg-like Kr (with $n \leq 9$) have been performed with a low-density tokamak plasma [17] and analyzed using theoretical data from the well-established RELAC code [18]. In the present work, the new relativistic multiconfiguration atomic structure code FAC [16] is used to identify emission features from F- to Al-like Kr in Kr cluster spectra. Experimental data have been collected in two spectral regions encompassing 4 – 2 (5.2 – 5.8 Å) and higher Ry-

dberg transitions (4.6 – 5.2 Å). Details of the experiment and a summary of the experimental results are given in Sec. II below. In Sec. III, a collisional-radiative model of O- to Si-like Kr that includes self-consistent opacity and hot electron effects is described and used to diagnose the size, density, temperature, and hot electron fractions of the cluster plasmas from the measured x-ray emission spectra. A discussion is given in Sec. IV and a summary is given in Sec. V.

II. EXPERIMENTAL SETUP AND RESULTS

The experiments were performed with the JAERI (Kyoto, Japan) 100 TW Ti:sapphire laser system, which is based on the technique of chirped pulse amplification. The laser was designed to generate 20 fs pulses centered at 800 nm at a 10 Hz repetition rate and is capable of producing focusing intensity up to 10^{20} W/cm^2 [19–21]. In this study, the amplified pulses were compressed to 30 - 500 fs by a vacuum pulse compressor yielding a pulse energy of 320 mJ. The pulses go through a regenerative amplifier and then through two double Pockels cells to reduce the prepulse, which comes before the main pulse by 10 ns. In this way, a contrast ratio of 5×10^{-6} between the intensity of the main pulse and the prepulse is achieved [20]. In a vacuum target chamber, the compressed pulses were focused by an $f/3$ Au-coated off-axis parabolic mirror. The measured spot size was 11 μm at $1/e^2$, which is 1.1 times larger than the diffraction limit. Approximately 64% of the laser energy was contained in the 11 μm Gaussian spot.

Figure 1 shows the experimental setup of the laser, gas jet nozzle and target, and spectrometer. The Kr clusters were produced by expanding a high pressure (20 to 30 atm) Kr gas into vacuum through a specially designed pulsed conical nozzle: the input and output diameters of the nozzle were 0.5 and 2.0 mm, respectively, and its length was 75 mm. The parameters of the nozzle were obtained from numerical modeling of a cluster target using the code developed at the Institute of Mathematical Modeling (RAS) [6, 15, 22]. By using this nozzle, Kr clusters with an average diameter around 1 μm can be produced at the laser focal spot, which was about 1.5 mm downstream from the nozzle. Such large clusters are less susceptible to destruction than the ≈ 0.1 μm Kr clusters produced in previous experiments [5].

Spatially resolved x-ray spectra were measured using a focusing spectrometer with spatial resolution (FSSR-2D) [23–25]. This spectrometer has been equipped with a spherically bent mica crystal (R=150 mm) and a vacuum-compatible x-ray CCD camera (DX420-BN, ANDOR), which was filtered with 8 μm of polypropelyne and 0.4 μm of Al. The spherically bent mica crystal was placed 381.2 mm from the plasma source and centered at $\lambda = 5.4$ Å (corresponding to the Bragg angle $\theta = 54.3°$ for the third reflection order of the mica crystal) in order to observe $4 - 2$ transitions in Kr. To observe higher

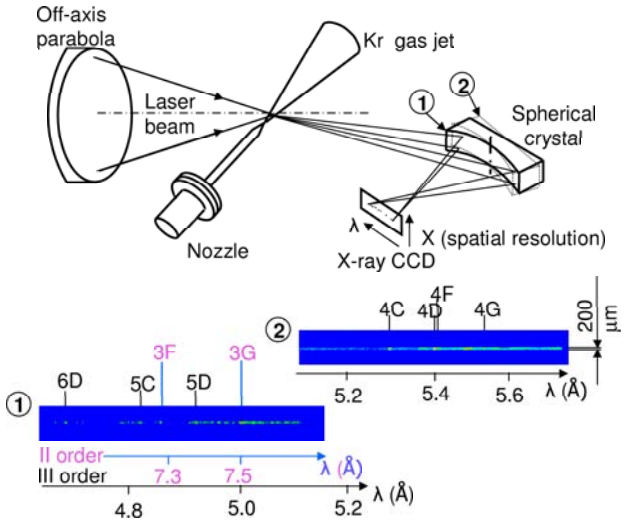

FIG. 1: Color online - Experimental setup, including laser, gas jet nozzle and target, and FSSR-2D spectrometer. Two alignments of the spherical mica crystal (numbered 1 and 2) were used to measure x-ray emission from two different spectral regions; spectra from these regions are given in the bottom panel. In alignment 1, the mica spectrometer captured $2p - 3s$ emission in second order as well as higher Rydberg emission.

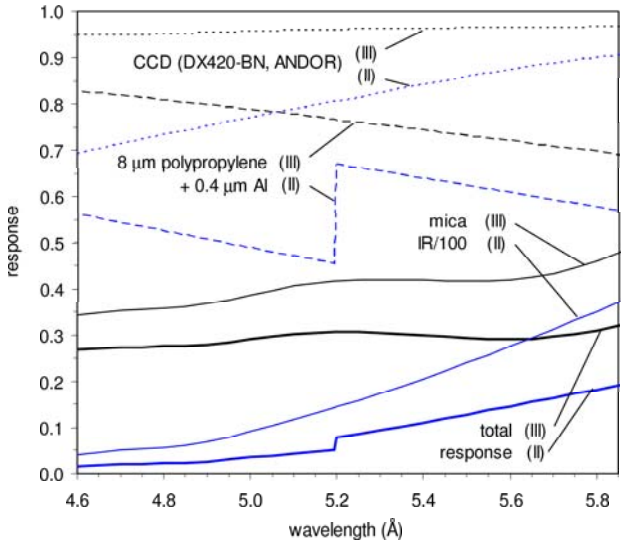

FIG. 2: Color online - Integrated reflectivities (IR) of mica in the second and third reflection orders. The plotted values are IR/100 taken from experimental data given in [26, 27]. Filter and CCD detector responses are also given for both reflection orders, along with the total response of the detection system.

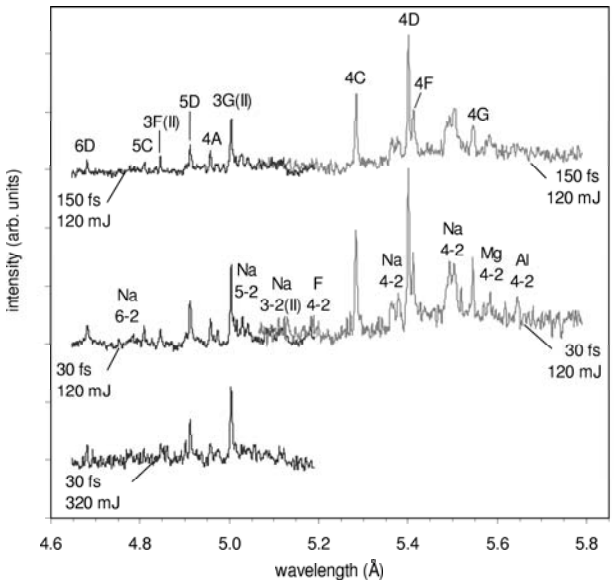

FIG. 3: Measured spectra of $n\ell - 2\ell'$ Kr emission from experiments with various laser energies and durations, with the incident laser intensities increasing from top to bottom. Ne-like Kr lines are labeled with their common designations and satellite features are labeled with their parent ion and the principal quantum numbers of the dominant transitions.

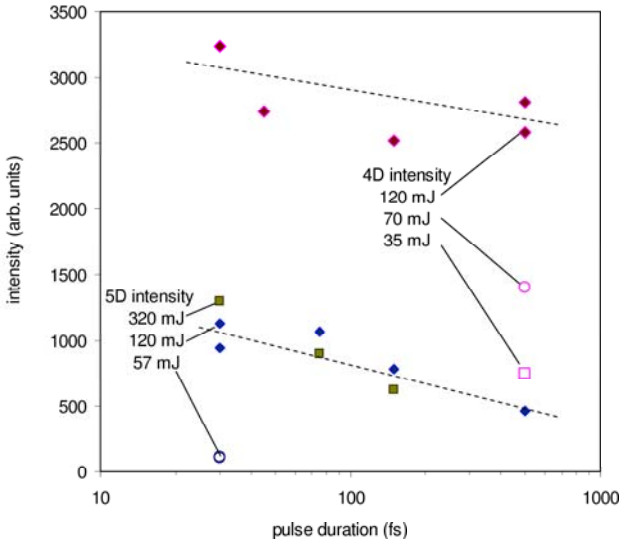

FIG. 4: Color online - Variation with laser pulse duration and energy of the measured intensities of Ne-like 4D and 5D lines.

Rydberg lines, the crystal was slightly shifted to 360 mm to obtain a central wavelength of $\lambda = 4.82$ Å (with a Bragg angle of $\theta = 46.5°$). The filter and CCD detector reponses (efficiencies) of the detection system and the integrated reflectivities of mica [26, 27] are given in Fig. 2 across the two spectral regions for both second and third order emission. Even though much of the second order emission is filtered out, some $2p - 3s$ emission is evident in the high-Rydberg spectral region (see Fig. 1).

The reflection plane of the spectrometer was oriented along the direction of the laser beam propagation to obtain spatial resolution in the transverse direction. The measured size of the emission zone in that direction was 200 – 250 μm. The emission zone in the direction of laser propagation was estimated to be between 1.0 and 1.5 mm. As the spectrometer crystal had a spherical shape and was placed on the Rowland circle, the spectral resolution was not sensitive to the size of the plasma source and approached the limit of the x-ray CCD camera detector ($\lambda/\Delta\lambda \approx 7000$).

Figure 3 shows measured spectra from each of the two alignments of the spectrometer for experiments with laser energies from 120 to 320 mJ and pulse durations from 30 to 150 fs. The relative spectral line intensities are proportional to the measured counts on the CCD. The top two spectra combine data from two experiments with the same laser parameters (120 mJ and durations of 150 and 30 fs) and different crystal alignments; the bottom spectrum shows only data in the high-Rydberg region for a 320 mJ, 30 fs laser pulse (no data was taken with the $4 - 2$ crystal alignment for these laser parameters). The wavelengths have been calibrated using theoretical values of Ne-like Kr lines calculated using the atomic structure code FAC [16]. The highly-resolved Ne-like lines are labeled with with their common designations nX, where n is the principal quantum number of the upper level and X specifies the transition type (nA and nB are $np - 2s$, nC and nD are $nd - 2p$, and nF and nG are $ns - 2p$). Other spectral features are labeled with their parent ions and the principal quantum numbers of the dominant transitions.

Although the laser intensity increases over an order of magnitude from top to bottom in Fig. 3, the measured spectra exhibit fairly little variation in their emission features. This near uniformity suggests that the plasma conditions attained in the clusters are only weakly affected by the laser parameters. Figure 4 shows experimental intensities of the 4D and 5D lines compiled from eighteen experiments with various laser energies and durations. The data have a fair level of reproducibility and exhibit a general trend of increasing emission intensity with increasing laser energy and decreasing laser duration. This dependence of x-ray emission intensity on the incident laser intensity, while rather weak, could be due either to variations in the plasma conditions reached in the clusters or to a variations in the number of emitting ions. These two possibilities are discussed in the modeling section below.

TABLE I: Configurations included in the collisional-radiative model and the number of fine-structure levels in each ion. Energies and rates coupling the levels have been calculated using the atomic structure code FAC [16]

Ion	Configuration	Num. Levels
O	$2s^2 2p^4$, $2s\ 2p^5$ $2s^2 2p^3 n\ell$, $2s 2p^4 n\ell$ $(n \leq 5)$	879
F	$2s^2 2p^5$, $2s 2p^6$ $2s^2 2p^4 n\ell$, $2s\ 2p^5 n\ell$ $(n \leq 5)$	480
Ne	$2s^2 2p^6$ $2s^2 2p^5 n\ell$, $2s\ 2p^6 n\ell$ $(n \leq 6)$	241
Na	$2s^2 2p^6 n\ell$ $(n \leq 6)$ $2s^2 2p^5 3\ell\ n\ell'$, $2s 2p^6 3\ell\ n\ell'$ $(n \leq 4)$ $2s^2 2p^5 3\ell\ nd$ $(n \leq 6)$	1410
Mg	$2s^2 2p^6 3\ell\ n\ell'$ $(n \leq 4)$ $2s^2 2p^5 3s\ 3\ell\ nd$ $(n \leq 4)$	707
Al	$2s^2 2p^6 3s^2 3p$ $2s^2 2p^6 3s^2 nd$ $(n \leq 4)$ $2s^2 2p^5 3s^2 3\ell\ nd$ $(n \leq 4)$	277
Si	$2s^2 2p^6 3s^2 3p\ 3\ell$ $2s^2 2p^6 3s^2 3\ell\ 4d$ $2s^2 2p^5 3s^2 3p\ nd$ $(n \leq 4)$	363

III. MODELED SPECTRA AND COLLISIONAL-RADIATIVE DIAGNOSTICS

The emission lines and features in the experimental Kr spectra were identified and calibrated with theoretical data calculated using the new relativistic multiconfiguration atomic structure code FAC [16]. The data includes level energies, radiative and Auger decay rates, collisional excitation and ionization cross sections, and radiative recombination cross sections for fine structure levels within O - through Si-like Kr. Table I lists the configurations and number of fine structure levels included in the calculations for each ion.

There are thousands of radiative transitions between levels in the listed configurations in the wavelength region from 4.6 – 5.8 Å. These have been separated according to their parent ion and plotted with intensities given by statistically-weighted radiative decay rates in Fig. 5. In this figure, the wavelength region is separated into high-Rydberg transitions (top) and $4-2$ transitions (bottom). Note that the radiative decay rates of similar transitions are quite uniform for ions from O- to Si-like Kr. For clarity, the $3-2$ features that appear in second order in the experimental spectra are not included in this figure; they consist mainly of the 3F and 3G Ne-like lines and associated Na- and Mg-like satellites.

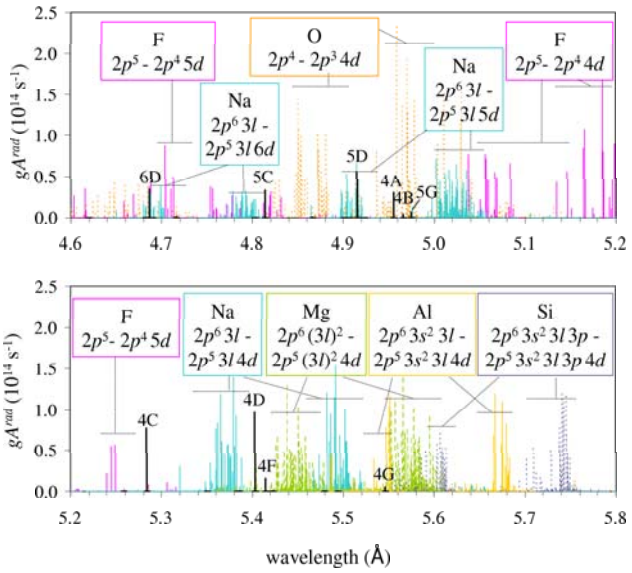

FIG. 5: Color online - Statistically weighted radiative decay rates (gA^{rad}) of high Rydberg $n\ell - 2\ell'$ (top) and $4\ell - 2\ell'$ (bottom) transitions from O- to Si-like Kr. The features are labeled with their parent ion and the dominant transition type.

A collisional radiative (CR) model based on the FAC data has been constructed to diagnose the cluster plasma conditions. A set of collisional-radiative rate equations are generated which include collisional excitation and de-excitation, collisional ionization, three-body recombination, dielectronic capture, Auger decay, radiative recombination, and radiative decay. The collisional rates are calculated using an electron distribution function characterized by an electron density n_e, a bulk electron temperature T_e, and a fraction of hot electrons f. Hot electrons are generated by resonant interactions between the main laser pulse and electrons that exist in a relatively cool plasma formed in the clusters by the laser prepulse [4–7]. and are modeled here by a narrow Gaussian distribution centered at 20 keV, following [5].

Level populations are obtained by solving the CR equations in the steady-state approximation. Opacity effects on the level populations are included self-consistently using the escape factor formalism, an iterative procedure which uses the level populations from one iteration to generate escape factors that modify the rate equations for the next iteration. The escape factors account for self-absorption and stimulated emission as photons from individual transitions are transported across the plasma.

Once level populations are determined, modeled spectra are constructed using Voigt profiles whose Doppler widths are dependent on the ion temperature (which is taken to be equal to T_e) and instrumental broadening and whose Lorentz widths are determined by the total rates of spontaneous and collisional depopulation from

the upper and lower levels of each transition. Using the slab approximation to account for opacity effects on line intensities and profiles, the modeled spectral intensity at a frequency ν is given by:

$$I(\nu) = \frac{j(\nu)}{\kappa(\nu)}\{1 - e^{-\kappa(\nu)d}\} \quad (1)$$

where $j(\nu)$ and $\kappa(\nu)$ are respectively the total emissivity and absorptivity of the plasma at the photon frequency ν, and d is the effective plasma size (for more details, see [28]). In the present case, where ≈ 1 μm dense clusters are surrounded by ≈ 10 μm of rarer plasma, d effectively includes only the cluster portion of the plasma, whose dimensions can be estimated to be $\approx 1/10^{th}$ the total plasma size.

The CR model has been used to calculate Kr emission across a wide range of plasma conditions. The emission intensity given above is then modulated by the detector response given in Fig. 2 in order to match the modeled spectra to measured data and thereby to diagnose the cluster plasma conditions. Following the results of [5], we assume the cool, rare plasma that surrounds the hot dense clusters makes relatively small contributions to the plasma emission and absorption. As will be shown below, the two reflection orders in the spectral region from 4.6 to 5.8 Å contain sufficient information to independently determine n_e, T_e, f, and the total size of the dense cluster plasma d.

Figure 6 shows modeled spectra at a variety of plasma conditions. The top spectrum illustrates emission that is fairly close to the measured spectra; the spectra below it show how changing particular parameters changes the modeled emission, bringing it out of agreement with the experimental data. The top spectrum has $n_e = 10^{22}$ cm^{-3}, $T_e = 300$ eV, $f = 1\%$, and includes the self-consistent opacity effects of 20 μm of plasma at that density. The spectrum just below it has the same conditions but is calculated in the optically thin limit; in this case the modeled 4F/4D ratio is far smaller than the experimental value. As shown in [5], the 4F/4D ratio is extremely sensitive to opacity effects and relatively insensitive to changes in other plasma parameters. Because the radiative decay rates of 4C and 4D are large compared to those of the higher Rydberg transitions, (see Fig. 5), those lines are more strongly affected by self-absorption at moderate optical depths. (The radiative decay rates of the $2p-3s$ transitions 3F and 3G are smaller than those of any $2p-nd$ transitions in this wavelength range, making those lines fairly insensitive to opacity effects.) By fixing the ratio 4F/4D to match the experimental data, the optical depth can be firmly established, and the product $n_e \times d$ can be fixed to simplify the determination of n_e, T_e, and f.

If the temperature, hot electron fraction, and $n_e \times d$ are held constant and the electron density is decreased to 10^{21} cm^{-3}, the third spectrum from the top in Fig. 6 is obtained. This spectrum has 3F and 3G lines which are much more intense than they are in the experimental

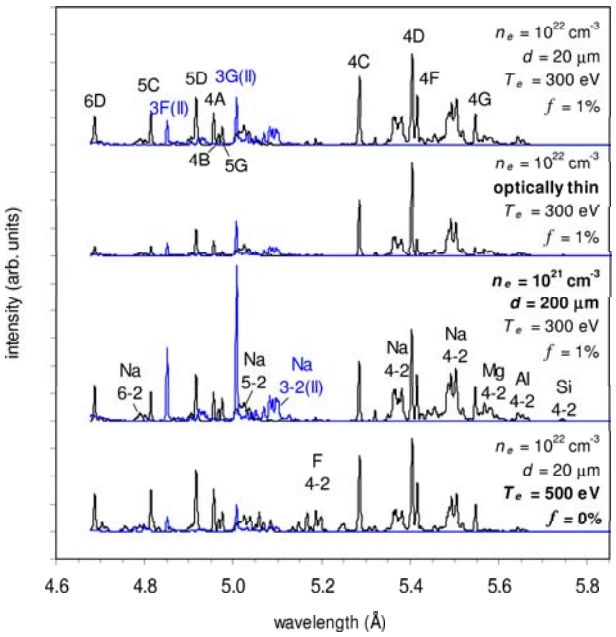

FIG. 6: Color online - Modeled spectra of $n\ell - 2\ell'$ Kr emission at various plasma conditions (including the total response of the detection system given in Fig. 2). Second $(3-2)$ and third order emission are given separately. The top spectrum has emission that broadly resembles the experimental data; the three spectra below it show how changes in the optical depth, density, and electron distribution affect the line intensities (the changed parameter in each case is given in bold).

data. The enhancement of the low-lying 3F and 3G line due to increased radiative cascades as electron densities decrease is a well-known effect [29] and has been used to diagnose electron densities in laser [9] and X pinch plasmas [30, 31]. Even considering variations in f (which can also affect the $3-2$ line intensities; see below), the electron density in the clusters must be above $\approx 5 \times 10^{21}$ cm^{-3} to match the experimental data.

When the density and $n_e \times d$ are held constant, and a single high-temperature ($T_e = 500$ eV) electron distribution function without hot electrons is used, then the bottom spectrum in Fig. 6 is obtained. The spectrum with hot electrons deviates from the high-temperature spectrum in several ways which are typically evident in both K- and L-shell spectra [32]: Including hot electrons leads to emission from a larger number of ions, amplifies certain high-energy lines within satellite features, and increases the intensities of the cascade-fed $3-2$ lines. These effects are sufficient to infer the presence of suprathermal electrons from the experimental spectra.

Figure 7 shows comparisons of the best-fit modeled spectra with experimental data. The top spectrum of Fig. 7, from Kr clusters irradiated by 120 mJ and 150 fs laser pulses, has a 4F/4D ratio that implies somewhat smaller opacity effects than were shown in Fig. 6. With

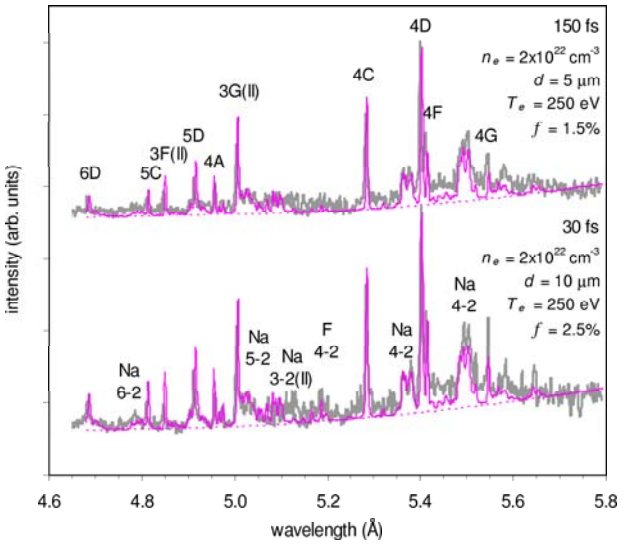

FIG. 7: Color online - Comparison of modeled spectra at the given plasma conditions with experimental data. The energy of the laser pulse in each case was 120 mJ and the pulse duration varies from 150 fs (top) to 30 fs (bottom).

an effective plasma size of 5 μm and an electron density of 2×10^{22} cm^{-3}, the 4F/4D ratio and the relative intensities of the $3-2$ lines to the $4-2$ and higher Rydberg emission are fit very well. With a bulk electron temperature of 250 eV and $f = 1.5\%$, the satellite features and charge state balance of the modeled spectrum match the experimental data quite closely.

The lower spectrum in Fig. 7 is also from clusters irradiated with 120 mJ of energy, but with a shorter pulse duration (30 fs). Although the incident laser intensity is five times larger in this case than in the 150 fs spectrum, the intensity of 4D increases by a factor of only ≈ 1.7. As previously noted, this relatively modest change in the emitted x-ray intensity could be caused either by changes in the plasma conditions or by changes in the number of radiating ions. Spectroscopic analysis suggests that both effects can pay a role; the spectrum from 30 fs laser pulse is best fit with the same temperature and density used to model the 150 fs spectrum, but with a larger fraction of hot electrons (2.5%) and a larger dimension (10 μm). These changes to the parameters not only increase the intensity of the modeled emission, but also increase the relative intensity of the F-like features near 5.2 Å and bring the 4F/4D ratio into agreement with the experimental data.

It should be noted that while the effects of the four parameters (T_e, f, n_e, and d) on the modeled line intensities are in principal distinguishable, they are sufficiently entangled that a determination of a demonstrably unique set of plasma conditions is quite difficult. This kind of multidimensional optimization problem is well-suited for treatment by, for example, genetic algorithms, which can efficiently explore a complex parameter space [28, 33].

IV. DISCUSSION

The modeled spectra given in Fig. 7 fit the experimental data quite well and give plasma parameters that are consistent with experimental constraints: Mathematical modeling of the Kr clusters estimates the cluster diameters to be ≈ 1 μm and the distance between clusters to be ≈ 10 μm. Since the clusters radiate after some attenuation by the laser prepulse but before they are completely destroyed, their effective size should be less than ≈ 20 μm, ($1/10^{th}$ the total plasma size of 200 μm; see Fig. 1). This is consistent with the diagnosed effective plasma size of $5-10$ μm. The energy required to form the radiating plasma at the diagnosed conditions is also consistent with experimental constraints: Taking the cluster plasma to be a cylinder of length 150 μm and diameter $5-10$ μm, and assuming a neutral plasma ($n_i = n_e/\langle Z\rangle$), there are $2-10\times10^{12}$ ions in the hot, dense cluster plasma at the diagnosed density. Since ≈ 30 keV ($\approx 5\times10^{-12}$ mJ) is required to ionize each Kr ion to the Ne-like charge state and heat the ionized electrons to the conditions in the diagnosed electron distribution, the cluster plasma requires $10-50$ mJ from the 120 mJ laser pulse.

The fairly weak variation of the measured x-ray intensities and spectroscopic features with order-of-magnitude changes in the incident laser intensity is a somewhat unexpected result, indicating that something other than the incident laser characteristics acts as a constraint on the x-ray generation and charge state balance in the cluster plasmas. This additional constraint may be the time scales available for ionization and x-ray production, which are limited by the time it takes the clusters to expand beyond the density at which collisions can efficiently excite and ionize the Kr ions. Indeed, while ionization from Na- to Ne-like Kr has a time scale of a few ps under the diagnosed plasma conditions, ionization of the stable Ne-like ion to F-like Kr takes about ten times longer. Since the large, $\approx 1\mu$m clusters dissipate in ≈ 2 ps, ionization stages much higher than Ne-like Kr may not be attainable even at ultrahigh laser intensities. However, since hot electrons are present in the cluster plasmas, inner-shell excitation of Ne-like Kr and surrounding ions may take place, and it would be interesting to look for K-shell transitions in future experiments. And since cluster size has a significant impact on the plasma evolution [milch01], the constraint imposed by collisional ionization may not apply if even larger clusters could be produced.

V. SUMMARY AND CONCLUSIONS

X-ray emission from $n\ell - 2\ell'$ transitions in F to Al-like Kr has been measured from Kr clusters irradiated with laser intensities up to 10^{19} W/cm^2. The incident laser intensities have been varied over an order of magnitude

by changing the energy and duration of the laser pulse, and a general trend of decreasing x-ray emission intensity with increasing laser pulse duration and decreasing laser energy has been observed. However, these trends are fairly small, and the emission features present in the measured emission spectra also change little over wide variations in laser intensity. The observations suggest that time constraints imposed by cluster expansion may limit the charge state balance regardless of the incident laser intensity.

The emission lines in the measured spectra have been identified and modeled using data from the new multiconfiguration relativistic atomic structure code FAC, which has proven to be a reliable theoretical tool. The conditions of the Kr cluster plasmas have been diagnosed using a collisional-radiative model based on the FAC data which includes self-consistent opacity and hot electron effects. The diagnosed electron densities are significantly higher than those in ns-laser and previous experiments performed with lower incident laser intensities and smaller clusters, as predicted in [5].

Acknowledgments

This work was supported in part by the Russian Foundation for Basic Researches (grant No. 02-01-00708), INTAS (grant No. 01-0233), and by Award No. RP1-2328-ME-02 of the U.S. Civilian Research & Development Foundation for the Independent States of the Former Soviet Union (CRDF). The work of S. H. and K. F. was performed under the auspices of the U.S. Department of Energy by University of California Lawrence Livermore National Laboratory under contract No. W-7405-Eng-48.

[1] A. McPherson, T. S. Luk, B. D. Thompson *et al.*, Phys. Rev. Lett. **72**, 1810 (1994).
[2] T. Ditmire, J. Zweiback, V. P. Yanovsky *et al.*, Nature (London) **398**, 489 (1999).
[3] H. M. Milchberg, S. J. McNaught, and E. Parra, Phys. Rev. E **64**, 056402 (2001).
[4] G. C. Junkel-Vives, J. Abdallah, Jr., F. Blasco *et al.*, Phys. Rev. A **66**, 033204 (2002).
[5] S. B. Hansen, A. S. Shlyaptseva, A. Y. Faenov *et al.*, Phys. Rev. E **66**, 046412 (2002).
[6] G. C. Junkel-Vives, J. Abdallah, Jr., T. Auguste *et al.*, Phys. Rev. E **65**, 036410 (2002).
[7] J. Abdallah, Jr., G. Csanak, Y. Fukuda *et al.*, Phys. Rev. A **68**, 063201 (2003).
[8] Y. Fukuda, K. Yamakawa, Y. Akahane *et al.*, Phys. Rev. A **67**, 061201(R) (2003).
[9] B. K. F. Young, B. G. Wilson *et al.*, J. Quant. Spectrosc. Radiat. Transfer **58** 991 (1997).
[10] K. B. Fournier, A. Ya. Faenov, T. A. Pikuz *et al.*, J. Quant. Spectrosc. Radiat. Transfer **81**, 167 (2003).
[11] K. B. Fournier, A. Ya. Faenov, T. A. Pikuz *et al.*, Phys. Rev. E **67**, 016402 (2003).
[12] J. Denavit and D. W. Phillion, Phys. Plas. **1**, 1971 (1994).
[13] C. A. Back *et al.*, Phys. Plas. **10**, 2047 (2003).
[14] K. B. Fournier *et al.*, Phys. Rev. Lett. **92**, 165005 (2004).
[15] A. S. Boldarev, V. A. Gasilov, and A. Ya. Faenov, Technical Phys., **49**, 388 (2004).
[16] M. F. Gu, Ap. J. **582**, 1241 (2003).
[17] J. E. Rice, K. B. Fournier, J. A. Goetz *et al.*, J. Phys. B: At. Mol. Phys. **33**, 5435 (2000).
[18] M. Klapisch, J. L. Schwob, B. S. Fraenkel, and J. Oreg, J. Opt. Soc. Am. **67**, 148 (1977).
[19] K. Yamakawa, M. Aoyama, S. Matsuoka *et al.*, Opt. Lett. **23**, 1468 (1998).
[20] Y. Fukuda, K. Yamakawa, Y. Akahane *et al.*, JETP Lett. **78**, 115 (2003).
[21] K. Yamakawa and C. P. J. Barty, IEEE J. Select. Topics Quantum Electron., **6**, 658 (2000).
[22] A. S. Boldarev, V. A. Gasilov, F. Blasco *et al.*, JETP Lett. **73**, 514 (2001).
[23] A. Ya. Faenov, S. A. Pikuz, A. I. Erko *et al.*, Phys. Scr. **50**, 333 (1994).
[24] I. Yu. Skobelev, A. Ya. Faenov, B. A. Bryunetkin *et al.*, JETP **81**, 692 (1995).
[25] B. K. Young, A. L. Osterheld, D. F. Price *et al.*, Rev. Sci. Instrum. **69**, 4049 (1998).
[26] S. G. Lee, J. G. Bak, Y. S. Jung *et al.*, Rev. Sci. Instr. **74**, 5046 (2003).
[27] G. Hölzer, O. Wehrhan, J. Heinisch *et al.*, Phys. Scr. **57**, 301 (1998).
[28] S. B. Hansen, Ph.D thesis, University of Nevada, Reno, 2003.
[29] J. Bailey, R. E. Stewart, J. D. Kilkenny *et al.*, J. Phys. B. **19**, 2369 (1986).
[30] A. S. Shlyaptseva, S. B. Hansen, V. L. Kantsyrev *et al.*, Phys. Rev. E. **67**, 026409 (2003).
[31] S. B. Hansen, A. S. Shlyaptseva, S. A. Pikuz *et al.*, Phys. Rev. E. (to be published).
[32] S. B. Hansen and A. S. Shlyaptseva, Phys. Rev. E. (to be published).
[33] I. E. Golovkin, R. C. Mancini, S. J. Louis *et al.*, J. Quant. Spectrosc. Radiat. Transfer **75**, 625 (2002).